

PAPER • OPEN ACCESS

A strategy for handling aberration in Spherical Neutron Polarimetry

To cite this article: Jacob Tosado *et al* 2019 *J. Phys.: Conf. Ser.* **1316** 012015

View the [article online](#) for updates and enhancements.



IOP | ebooks™

Bringing you innovative digital publishing with leading voices to create your essential collection of books in STEM research.

Start exploring the collection - download the first chapter of every title for free.

A strategy for handling aberration in Spherical Neutron Polarimetry

Jacob Tosado,^a Wangchun Chen^{b c} and Efrain E. Rodriguez^a

^aDepartment of Chemistry & Biochemistry, University of Maryland, College Park, MD 20742.

^bNIST Center for Neutron Research, National Institute of Standards and Technology, 100 Bureau Drive, Gaithersburg, MD 20899.

^cDepartment of Materials Science and Engineering, University of Maryland, College Park, MD 20742.

E-mail: jtosado@umd.edu

Abstract. We present a strategy for identifying and correcting for aberration effects in Spherical Neutron Polarimetry. The transformation of the neutron beam polarization vector due to scattering from a material is determined with Spherical Neutron Polarimetry. This neutron scattering technique measures the three cardinal components of the scattered polarization for any chosen cardinal direction of the incident polarization for a given Bragg reflection. As a consequence, the instrumentation required for this technique is desired to be capable of measuring the three-dimensional polarization vector over the sphere. As with all instrumentation, the field of measurement is subject to aberration which must be characterized.

1. Introduction

Spherical Neutron Polarimetry (SNP) is a neutron scattering technique that measures the nine elements of the polarization property tensor of a material [1]. These nine elements are derived from the three-dimensional neutron beam polarization vector with Cartesian components $P_j = (I_+ - I_-)/(I_+ + I_-)$, for $j = 1, 2$ or 3 corresponding to X, Y or Z. The terms, I_{\pm} , correspond to the measured intensity of the $\pm 1/2$ spin eigenstates of the neutron angular momentum in the j^{th} direction. This measurement technique was first fully realized in 1989 at the Institut Laue-Langevin [2] and has since been revised, [3] expanded upon [4, 5] and developed elsewhere [6]. Figure 1 illustrates in a three step process the general layout of SNP. In the first step, the polarization direction of the incident polarized neutron beam is set to one of the j^{th} Cartesian directions. In the second step, this oriented polarized beam scatters, through Bragg reflection from a crystal, which changes the neutron beam's initial momentum, \mathbf{k}_1 , to some final momentum, \mathbf{k}_2 . In the third step, for a given Bragg reflection, the axis of measurement is set to measure one Cartesian component of the scattered neutron beam. Orienting and measuring all possible directional combinations yields the nine component polarization property tensor for that material at a specific Bragg reflection.

The Cartesian axis of measurement and orientation is fixed relative to the scattering vector, \mathbf{Q} , which specifies a Bragg reflection and is defined as the change in momentum between the incident and scattered neutron beams (i.e., $\mathbf{Q} = \mathbf{k}_2 - \mathbf{k}_1$). We call this frame of reference the Q-frame. To easily move a neutron detection apparatus about a crystal and thereby measure



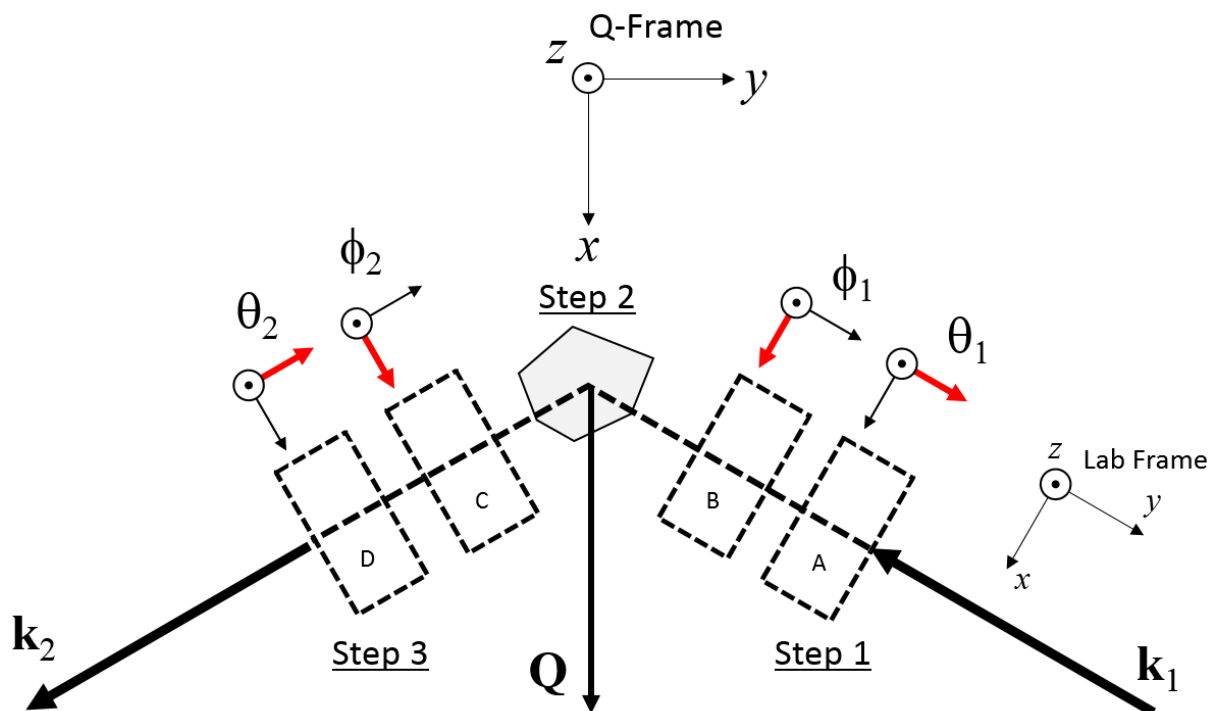


Figure 1. Coordinate system of the SNP setup as seen from the Q-frame. Here, the XY-plane is the scattering plane. The relative placement of polarization control instrumentation is outlined with boxes. Adjacent to each box, the respective local coordinate system and local control parameter are depicted. For each local coordinate system, the axis of rotation for the control parameter is highlighted in red. The letters distinguish the instrumentation as follows: **A)** Local rotation about the y_1 axis, $R_{y_1}(\theta_1)$ **B)** Local rotation about the x_1 axis, $R_{x_1}(\phi_1)$ **C)** Local rotation about the x_2 axis, $R_{x_2}(\phi_2)$ **D)** Local rotation within the XZ-plane, $B_{xz}(\theta_2)$

different \mathbf{Q} , the possible directions of \mathbf{Q} are typically restricted to rotations about a single axis fixed in the lab frame. The lab frame may be thought of as being aligned with, \mathbf{k}_1 , the direction of the incident neutron beam. The resulting plane through which \mathbf{Q} rotates defines what is called the scattering plane.¹ The Cartesian directions are then typically labeled X, Y and Z where X is parallel to \mathbf{Q} , Z is vertical and perpendicular to the scattering plane and, Y completes the orthogonal set. Upon scattering, the neutron beam's initial state polarization is transformed by interacting with the magnetic structure of the crystal to some final state polarization. That transformation is defined by the Blume-Maleyev tensor [7].

2. Calibration

The instruments that orient the incident polarization and set the direction of the measurement axis each have local independent coordinate systems. Through calibration, the local coordinate system of each instrument is transformed into the Q-frame. As such, calibration requires the precise mutual alignment of each coordinate system and the precise characterization of distortions inherent within the SNP apparatus. Each SNP component device(s) can be identified with respect to the polarization degree of freedom that it controls and/or measures. As a result,

¹ Throughout this article we generally assume that the scattering plane is level with the floor of the laboratory. This is an important assumption in that it places real restrictions on the overall geometry of an SNP apparatus which naturally influences the potential distortion in the measurement.

there are four main devices corresponding to four degrees of freedom: two degrees for the incident beam and two degrees for the scattered beam, which must be mutually aligned. To understand alignment one can describe the measurement of a single component, P_j , of the polarization vector in terms of the rotation of an initial state polarization vector and its dot product with the measurement axis in the Q-frame. This is given by the relationship,

$$P_j = \mathbf{B}(\Theta_2, \Phi_2) \cdot T R(\Theta_1, \Phi_1) \mathbf{P}_o \quad (1)$$

Here \mathbf{P}_o is the initial state polarization, T is the Blume-Maleyev tensor, $R(\Theta_1, \Phi_1)$ is the net rotation of the initial state polarization by the instrumentation and $\mathbf{B}(\Theta_2, \Phi_2)$ is the axis of measurement. The spherical coordinates $\Theta_{1,2}$ and $\Phi_{1,2}$ are angles about the Q-frame Y and X axes, respectively. Implicitly, T , Θ_1 , Φ_1 , Θ_2 and Φ_2 are all dependent on \mathbf{Q} . For simplicity we will first consider one value of \mathbf{Q} and later discuss other directions. From Equation 1 the three steps of Figure 1 can be distinguished mathematically as,

- | | | |
|---------|------------------------------------|---|
| Step 1. | $R(\Theta_1, \Phi_1) \mathbf{P}_o$ | Directing the incident polarization |
| Step 2. | T | Scattering from a crystal |
| Step 3. | $\mathbf{B}(\Theta_2, \Phi_2)$ | Measurement of the scattered polarization |

The first part in calibration is to remove effects due to magnetic scattering from a crystal so as to isolate the character of the apparatus. This can be achieved by either removing the crystal from the SNP apparatus altogether and measuring the polarization of the purely transmitted beam or by measuring the scattered polarization of a pure nuclear Bragg peak. In either case, having all effects resulting from magnetic scattering properly removed will reduce T to the identity operator.

To understand the calibration of each component instrument we first decompose the rotation operator, $R(\Theta_1, \Phi_1)$, into three operators: $R_{in}(\mathbf{Q})$, $R_{y_1}(\theta_1)$ and $R_{x_1}(\phi_1)$ where, $R(\Theta_1, \Phi_1) = R_{in}(\mathbf{Q})R_{x_1}(\phi_1)R_{y_1}(\theta_1)$. Here, $R_{y_1}(\theta_1)$ and $R_{x_1}(\phi_1)$ represent a rotation about the local y_1 and x_1 axes, respectively, and $R_{in}(\mathbf{Q})$ represents the net transformation into the Q-frame. In Figure 1 the relative orientations of the local axis as seen from the Q-frame are depicted. The measurement axis decomposes likewise into three operators: $\mathbf{B}_{xz}(\theta_2)$, $R_{x_2}(\phi_2)$, and $R_{out}(\mathbf{Q})$ where $\mathbf{B}(\Theta_2, \Phi_2) = \mathbf{B}_{xz}(\theta_2)R_{x_2}(\phi_2)R_{out}(\mathbf{Q})$. Here $\mathbf{B}_{xz}(\theta_2)$ is a local planar measurement field in the XZ-plane, $R_{x_2}(\phi_2)$ is a local rotation of the scattered polarization into that field, and $R_{out}(\mathbf{Q})$ is the net transformation out of the Q-frame. To simplify matters further, we only consider the transmitted beam method for calibration such that T , $R_{in}(\mathbf{Q})$ and $R_{out}(\mathbf{Q})$ each reduce to the identity operator.² The measured polarization of the purely transmitted beam is now,

$$P_j = \mathbf{B}_{xz}(\theta_2)R_{x_2}(\phi_2) \cdot R_{x_1}(\phi_1)R_{y_1}(\theta_1) \mathbf{P}_o \quad (2)$$

From this Equation we can define two domains on either the incident polarization or on the measurement of the scattered polarization. The first is the domain of control, which describes all possible orientations of the incident polarization,

$$\mathbf{S}_{con}^2 = \{(\theta_1, \phi_1) \mid 0 \leq \theta_1 \leq 2\pi, 0 \leq \phi_1 \leq \pi\} \quad (3)$$

The second is the domain of measurement, which describes all possible orientations of the measurement axis \mathbf{B} ,

$$\mathbf{S}_{mes}^2 = \{(\theta_2, \phi_2) \mid 0 \leq \theta_2 \leq 2\pi, 0 \leq \phi_2 \leq \pi\} \quad (4)$$

² The operators R_{in} and R_{out} are a very simple way of mathematically visualizing the coordinate transformation of $\theta_{1,2}$ and $\phi_{1,2}$ into the Q-frame.

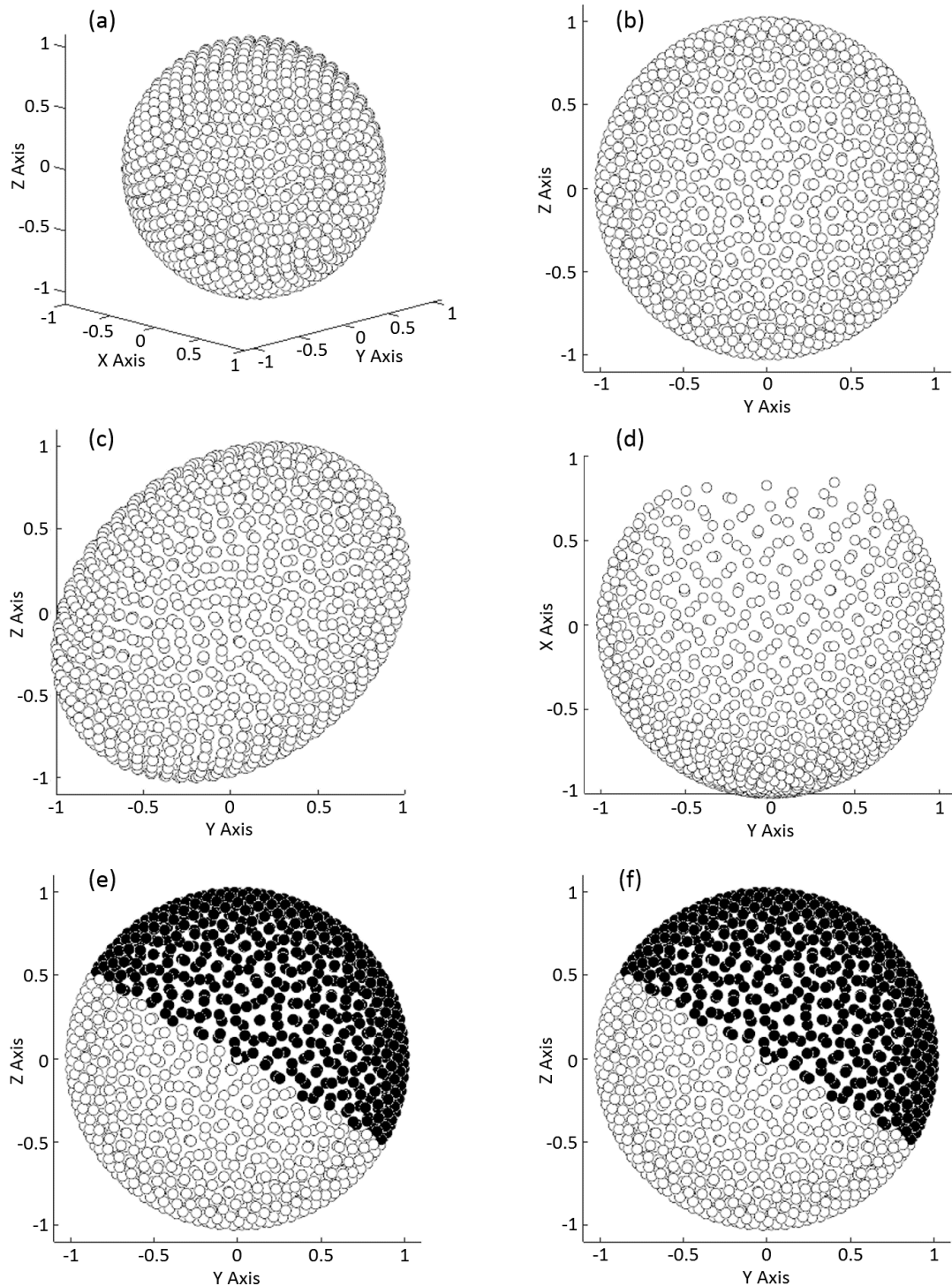


Figure 2. Simulated SNP measurement field. (a) and (b) Measurement field with no misalignment. (c) Misalignment applied by setting $\alpha_1 = 30^\circ$ (d) Misalignment applied by setting $\alpha_2 = 30^\circ$ (e) Misalignment applied by setting $\beta_1 = 30^\circ$ (f) Misalignment applied by setting $\beta_2 = 30^\circ$. In Figures (e) and (f) the data is segregated into two hemispheres with black and white face circles. This is to show clearly the effect of misalignment, which is identical in these two cases.

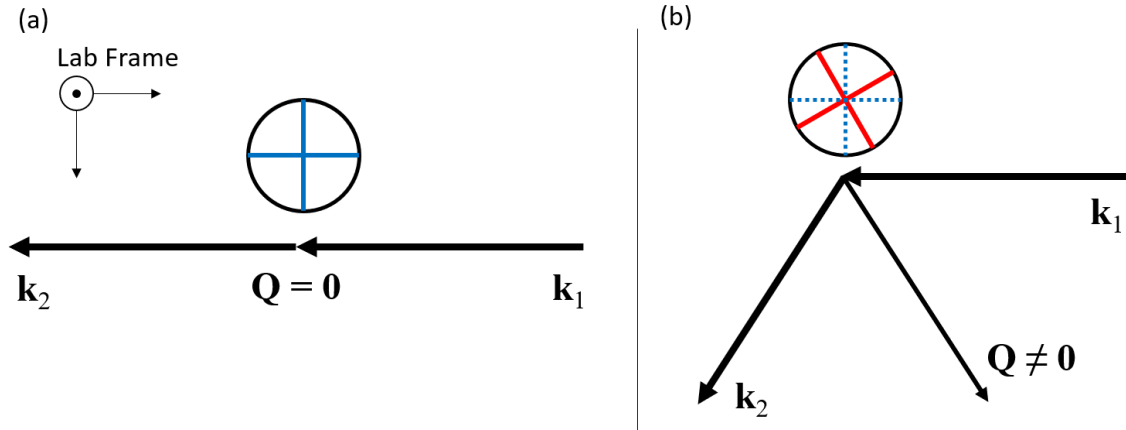


Figure 3. Orientation of the Q-frame for different values of \mathbf{Q} as seen in the lab frame. (a) The transmission configuration during calibration and, (b) Crystal measurement. The blue cross (solid & dashed) indicates the Q-frame orientation for $\mathbf{Q} = 0$ and the red cross indicates the Q-frame orientation for $\mathbf{Q} \neq 0$.

Table 1. (Left) The opposing angles required for measuring the j^{th} vector component over the control domain. (Right) The opposing angles required for measuring the j^{th} vector component over the measurement domain.

	θ_2	ϕ_2		θ_1	ϕ_1
X	$\pi/2$	0	X	$\pi/2$	0
Y	0	$\pi/2$	Y	0	$-\pi/2$
Z	0	0	Z	0	0

For each element of either \mathbf{S}^2_{con} or \mathbf{S}^2_{mes} , Equation 2 will produce a vector $\mathbf{P} = \sum_j P_j \hat{\mathbf{e}}_j$ from three cardinal orientations corresponding to $j = 1, 2$ or 3 of the two opposing angles. The angles of these three opposing orientations for both the control and measurement domains are shown in Table 1. As an example, a measurement of some vector \mathbf{P}_G , from the control domain \mathbf{S}^2_{con} , first requires the setting $(\theta_1, \phi_1)_G$ to access the G^{th} point in that domain. Then one must independently measure the X, Y and Z components by setting (θ_2, ϕ_2) according to the Table 1 values for the \mathbf{S}^2_{con} domain. When properly aligned, the resulting range of vectors, \mathbf{P} , for each domain ideally form a spherical field of radius P_o centered at the origin. Figures 2(a) and (b) illustrate a three-dimensional plot of the ideally aligned perfectly spherical measurement field resulting from the \mathbf{S}^2_{mes} domain. In this context, misalignment can now be characterized by the Q independent phases $\alpha_1, \beta_1, \alpha_2$ and β_2 , which add to the local control coordinates, i.e.,

$$P_j = \mathbf{B}_{xz}(\theta_2 + \alpha_2)R_{x_2}(\phi_2 + \beta_2) \cdot R_{x_1}(\phi_1 + \beta_1)R_{y_1}(\theta_1 + \alpha_1)\mathbf{P}_o \quad (5)$$

From Figure 2 one can see how the addition of these phases distorts the sphere. Figure 2(c) shows the resulting distortion in the measurement field (or equivalently the control field) when $\alpha_1 = 30^\circ$. From Figure 2(d) the distortion is entirely different when the same misalignment angle, $\alpha_2 = 30^\circ$, is applied. In contrast to these, Figures 2(e) and (f) show a tilting of the spherical field when the same 30° misalignment is applied to either β_1 or β_2 separately. In all of these cases, switching the sign of the misalignment mirrors the distortion and, combinations of misalignment superpose. These phases can be deduced by an iterative comparison of measured data with

simulation. The phases are then corrected for by electromechanical means within the hardware until the apparatus is well described by Equation 2 alone. We therefore define misalignment to be any distortion in either the control or measurement fields that is well described by Equation 2.

Physically, alignment through measuring either the control or measurement fields acts to maximize the transmission of polarization through the SNP apparatus along the cardinal directions of the \mathbf{Q} -frame. The control and measurement fields, while both spherical, differ in that they describe different aspects of the SNP functionality. For example, consider Figure 3. Here, two values of \mathbf{Q} in the lab frame are depicted, one for $\mathbf{Q} = 0$ and one for $\mathbf{Q} \neq 0$. For both values of \mathbf{Q} the orientation of the corresponding spherical field is also depicted. The $\mathbf{Q} = 0$ case (Figure 3(a)) was used for alignment and is described by Equation 2. During the measurement of a crystal, \mathbf{Q} will most likely be non-zero and the resulting \mathbf{Q} -frame will be rotated relative to the \mathbf{Q} -frame used for alignment (refer again to Figure 3(b)). Consider that at most six points of the measurement field are needed for any given \mathbf{Q} . In the lab frame, this amounts to the vertical poles and a great circle within the scattering plane of the measurement field. Practically, only these regions of the measurement field need to be well described by Equation 2. This is not so for the control field. Nuclear-magnetic scattering, at values of $\mathbf{Q} \neq 0$, would result in a scattered polarization directed away from the \mathbf{Q} -frame cardinal axes [8]. If the control field is distorted in that direction and is fixed to the lab frame, then that distortion will propagate to any polarization measurement when the direction of scattered polarization coincides with that distortion, regardless of how spherical the measurement field is.

To emphasize the difference between the measurement and control fields we must first consider two other forms of distortion in addition to misalignment, noise and aberration. Noise we characterize as the expected variation in the spherical field due to the compounded Poisson error of the neutron detection process [9]. Aberration, in contrast, we define as distortion which is greater than the noise and is not well described by misalignment (i.e., Equation 2). As an example of noise, first consider Figures 4(a) and (c) which shows a simulation of 1024 discrete measurements on the \mathbf{S}^2 domain where Figures 4(b) and (d) are respective Mollweide projections of Figures (a) and (b). We use the Mollweide projection to visually retain the relative proportionality of the point distribution when compared to the three-dimensional plots [10]. In Figures 4(a) and (b) the average noise level is twice as large as the angular sampling period (i.e., the average angular distance between points in \mathbf{S}^2). Consequently, the noise is the dominant signal and the sampling period satisfies the Nyquist-Shannon sampling limit [11], meaning that this spherical field is noise limited. The noise level, displayed in Figures 4(c) and (d), has been reduced by an order of magnitude but the sampling period is unchanged (i.e., an equivalent 1024 points have been used). In this case, the noise fluctuation is small and features resulting from any other distortion may only be resolved if the Nyquist-Shannon sampling limit is met. This means that the spherical field for this reduced noise level is now Nyquist-Shannon limited. In other words, the angular resolution provided in Figures 4(c) and (d) is now adequate to resolve aberration in the spherical field occurring at large enough angular scales.

Now consider an example of aberration in the control field, for $\mathbf{Q} = 0$, depicted in Figures 5(a) and (b). We imagine this type of aberration being brought about by artifacts in either the laboratory or the sample environment. By mapping such an aberration, as in Figure 5(b), real space correlation to known artifacts would potentially allow the source of the aberration to be identified and removed. Figure 5 is a simulation where the noise level here is equivalent to that used in Figures 4(c) and (d). This simulated aberration appears in a decrease in polarization within the upper octant of the control field. Figure 5(b) shows that the aberration is localized within that octant and does not intersect the cardinal planes. If this aberration is now fixed relative to the lab frame then, for some value of $\mathbf{Q} \neq 0$, the cardinal planes would intersect it resulting in a loss of transmitted polarization. Figure 5(c) through (e) show the projections

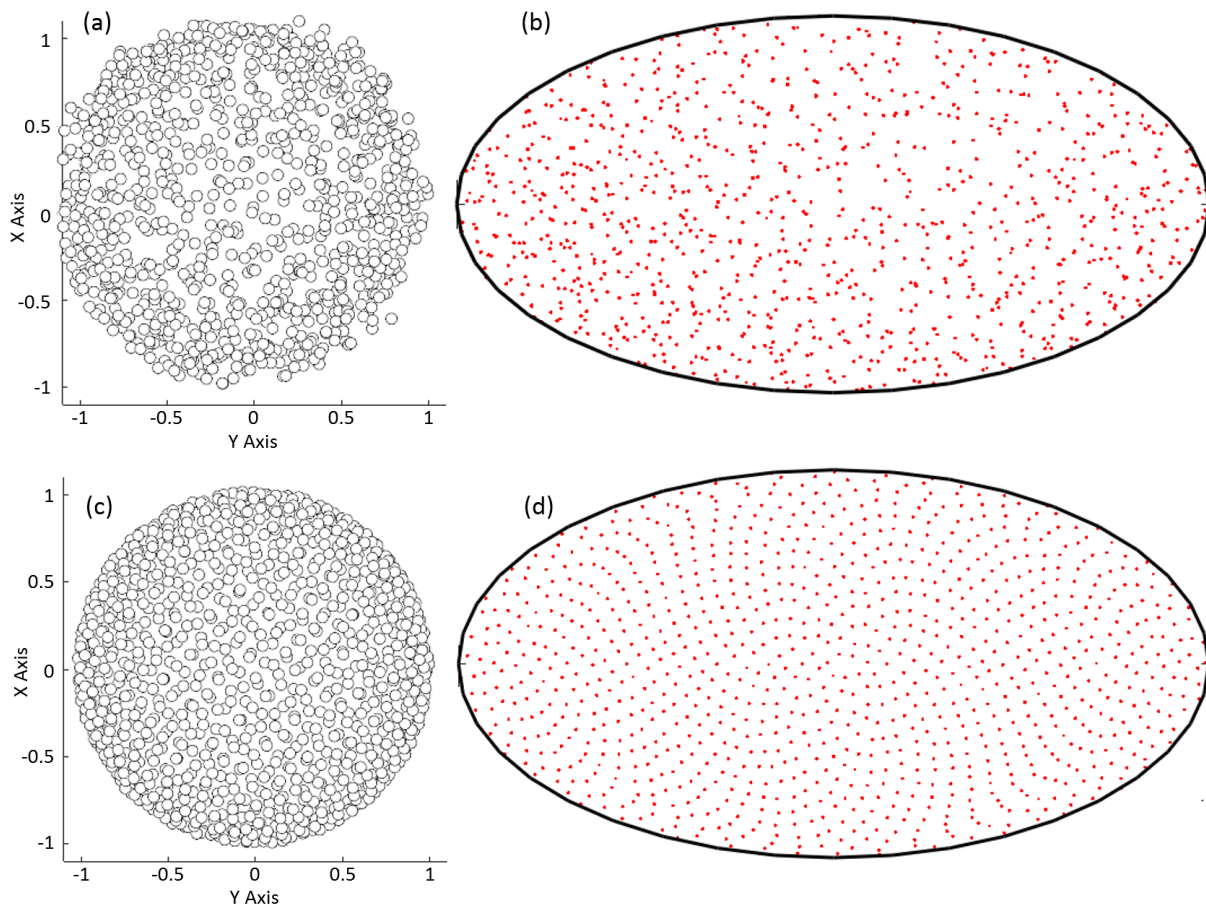


Figure 4. Simulation of the spherical field for two noise levels plotted in 3D and as a 2D Mollweide projection. (a) and (b) Noise Limited Data where the noise level is twice a large as the sampling period. (c) and (d) Nyquist Limited Data where the noise level is much smaller than the sampling period.

of this aberrated control field onto the cardinal planes for $\mathbf{Q} = 0$. Since the polarization in each projection follows the great circle (outlined in black) of that respective projection plane, the resulting measurement field will appear to be undistorted. Again, this is because only the undistorted X, Y and Z directed polarizations of the control field are used in constructing the measurement field. Therefore only a spherical measurement of the control field through the aberrated region will fully account for that distortion.

To characterize the type of aberration depicted in Figure 5 we now explore a strategy that involves expanding the measurement field in terms of a finite series of spherical harmonics. Techniques similar to this have been used to model three-dimensional data for Computer Generated Imaging (CGI) [12].

$$P(\theta, \phi) = \sum_{n=0}^N \sum_{m=-n}^n \epsilon_{nm} Y_{nm}(\theta, \phi) \quad (6)$$

Equation 6 describes an expansion of the magnitude of the measured polarization on the \mathbf{S}^2 domain in terms of the spherical harmonics $Y_{nm}(\theta, \phi)$ with coefficients ϵ_{nm} for degree n and order m . Here the maximum degree, N , is determined by the total number of measurements

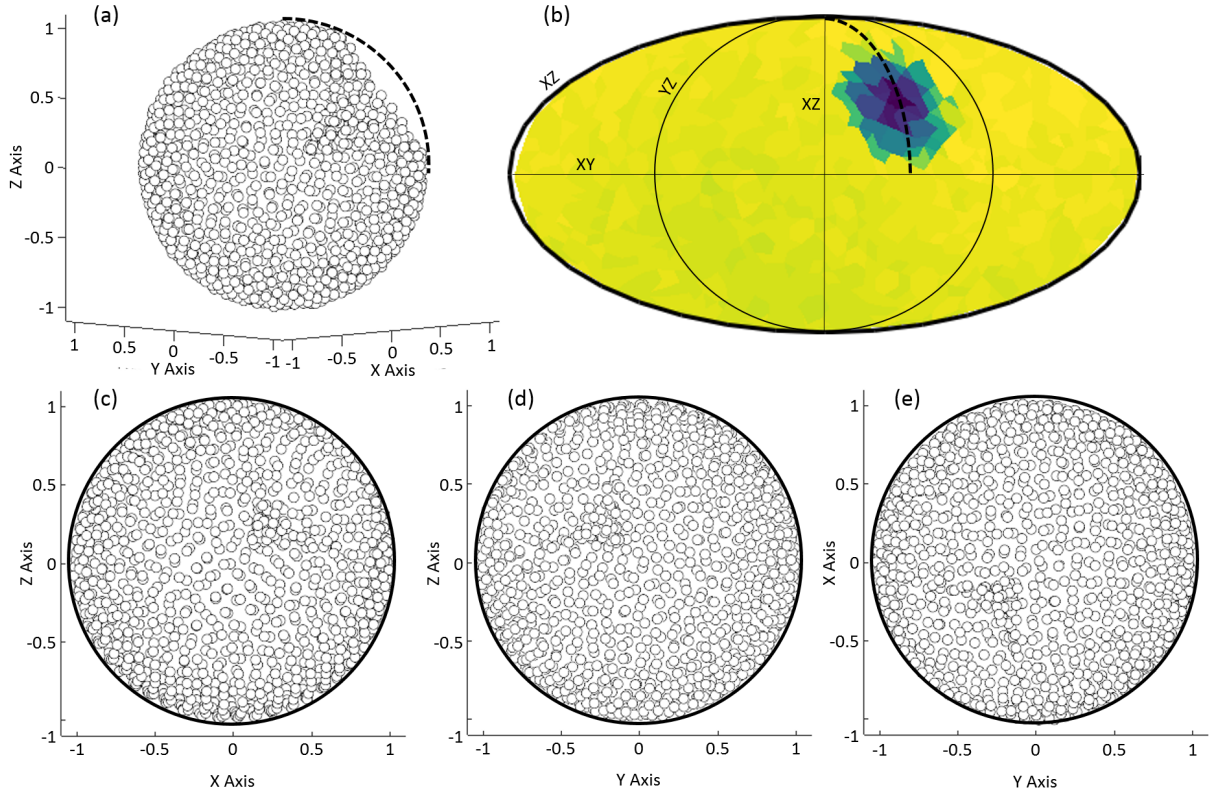


Figure 5. Simulated aberration. The noise level is equivalent to Figure 4(b). (a) A three-dimensional plot showing a decrease of polarization relative to the control field. The dotted line indicates the undistorted polarization. (b) Mollweide projection of of the simulation showing that the distortion is localized within one octant of the sphere. Here arcs and lines indicate great circles and are labeled according to the respective plane that contains them. The dotted line of (a) is also shown. (c-e) Projections of the simulation onto the planes labeled in (b). Great circles act as a guide for the eye.

taken, similar to discrete Fourier analysis.

To apply this expansion, we first begin by correcting for angular aberration. Angular correction serves to regularize the spherical field for harmonic decomposition by Equation 6. The operation we suggest here is a simplified form of image warping and we refer to Wolberg (1990) , for a more in depth treatment [13]. This is a procedure which first involves calculating the set of spherical angles, $\{A_k, B_k\}$, from the set of vectors, $\{\mathbf{P}_k\}$. Each A_k and B_k then correspond to the expected angles, a_k and b_k , set by the instrumentation such that the resulting angular aberration is the respective difference,

$$\delta_k = A_k - a_k, \quad \rho_k = B_k - b_k \quad (7)$$

To later apply this to an arbitrary measurement we may linearly interpolate between angles such that for an arbitrary pair of measured angles, (γ, ζ) , which, for example, are in the intervals, $A_k \leq \gamma \leq A_{k+1}$ and $B_k \leq \zeta \leq B_{k+1}$, the calculated aberration for those angles is,

$$\Delta_\delta = \left| \frac{\gamma - A_k}{A_{k+1} - A_k} \right| (\delta_{k+1} - \delta_k) + \delta_k \quad (8)$$

$$\Delta_\rho = \left| \frac{\zeta - B_k}{B_{k+1} - B_k} \right| (\rho_{k+1} - \rho_k) + \rho_k \quad (9)$$

The corrected angles for an arbitrary measurement are then,

$$\Theta = \gamma - \Delta_\delta \quad (10)$$

$$\Phi = \zeta - \Delta_\rho \quad (11)$$

With the angular distortion removed, correcting for radial distortion is more straight forward. This is accomplished by describing the set of magnitudes, $\{P_k\}$, of the calibration data with Equation 6. A correction to an arbitrary measurement, $P_{measured}$, with spherical angles Θ and Φ is then,

$$C(\Theta, \Phi) = \sum_{n=1}^N \sum_{m=-n}^n \epsilon_{nm} Y_{nm}(\Theta, \Phi) \quad (12)$$

such that,

$$P_{corrected} = P_{measured} - C \quad (13)$$

The corrected polarization described in Equation 13 is subject to the innate Poisson error of the calibration data, $\{\mathbf{P}_k\}$, and this error will propagate to the corrected polarization. We suggest that the error in $\{\mathbf{P}_k\}$ be kept to a level much smaller than that used for routine measurement.

3. Discussion

Thus far we have considered the limited case where both the control and measurement fields, measured at one value of \mathbf{Q} , are fixed to the lab frame and are therefore \mathbf{Q} -dependent. This dependency is described simply by a rotation of these fields about the Z-axis (Figure 3). In this sense, calibration requires characterization of one control and measurement field. Experimentally, we estimate that the measurement of a single spherical field would take about 20 hours for a neutron flux on the order of $2 \times 10^6/\text{cm}^2/\text{s}$. The simplicity of this kind of \mathbf{Q} -dependency may be somewhat of an ideal since the modern SNP apparatus requires movement of instrumentation in the lab frame to measure different \mathbf{Q} . An actual \mathbf{Q} -dependency may be more complicated requiring field characterization at more than one \mathbf{Q} . In any case, the strategy we have outlined for characterization of the control and measurement fields would not change.

Finally, it must be pointed out that SNP calibration typically involves only measuring vector components along great circles within the control and measurement fields [4, 14, 5]. To date, there has been no attempt to characterize variation in an SNP apparatus over a spherical domain. As a result, it is not clear in what context aberration will significantly affect SNP measurements. For minor aberration in the control field, that is an aberration on the order of 2% above the noise, we expect aberration to have the potential of severely effecting measurements of weak nuclear-magnetic reflections. For these reflections, the nuclear component may be significantly stronger than the magnetic and, any loss in intensity could wrongfully suggest that the signal is purely nuclear.

Acknowledgments

Certain commercial entities, equipment, or materials may be identified in this document in order to describe an experimental procedure or concept adequately. Such identification is not intended to imply recommendation or endorsement by the National Institute of Standards and

Technology, nor is it intended to imply that the entities, materials, or equipment are necessarily the best available for the purpose. The work utilized facilities supported in part by the National Science Foundation under Agreement No. DMR-1508249.

This work was supported by the Department of Energy, Basic Energy Sciences Project, Award DE-SC0016434.

References

- [1] Brown P J, Nunez V, Tasset F, Forsyth J B and Radhakrishna P J 1990 *Phys.: Condens. Matter* **2** 9409
- [2] Tasset F 1989 *Physica B* **156** 627
- [3] Lelievre-Berna E et al. 2005 *Physica B* **356** 141-5
- [4] Hutanu V, Meven M, Masalovich S, Heger G and Roth G 2011 *Journal of Physics: Conference Series* **294** 012012
- [5] Takeda M, Nakamura M, Kakurai K, Lelievre-Berna E, Tasset F and Regnault L-P 2005 *Physica B* **356** 136
- [6] Janoschek M, Klimko S, Gahler R, Roessli B and Boni P 2007 *Physica B* **397** 125
- [7] Blume M 1963 *Physical Review* **133** 1366
- [8] Brown P J 2006 *Neutron Scattering from Magnetic Materials* ed T Chatterji (The Netherlands: Elsevier) chapter 5 pp. 215-244
- [9] Lelievre-Berna E, Brown P J, Tasset F, Kakurai K, Takeda M and Regnault L-P 2007 *Physica B* **397** 120-4
- [10] Snyder J P *Map Projections - A Working Manual* (Washington: United States Government Printing Office) chapter 31 pp. 249-252
- [11] Shannon C E 1998 *Proceedings of the IEEE* **86** 447-57
- [12] Basri R and Jacobs D W 2003 *IEEE Transactions on Patter Analysis and Machine Intelligence* **25** 218-33
- [13] Wolberg G 1990 *Digital Image Warping* (Wiley-IEEE Computer Society Press)
- [14] Wang T, Parnell S R, Hamilton W A, Li F, Washington A L, Baxter D V and Pynn R 2016 *Review of Scientific Instrument* **87** 033901